A shared observation shields collective fluctuations while preserving local independence

Cite as: AIP Advances 16, 115017 (2026); doi: 10.1063/5.0355816
Submitted: 12 August 2026 • Accepted: 15 October 2026 •
Published Online: 5 November 2026

View Online Export Citation CrossMark

Hu Cang[a]

AFFILIATIONS

Department of Developmental and Cell Biology, University of California, Irvine, California 92697, USA

[a]Author to whom correspondence should be addressed: cangh@uci.edu

ABSTRACT

As a liquid approaches its glass transition, its dynamics turns heterogeneous: mobile and immobile regions coexist, and the four-point susceptibility χ_4 that quantifies this heterogeneity grows sharply. However, collective signals such as tracer trajectories, overlap functions, or mean fields are generated by the very particles they monitor. Here, we compute exactly what conditioning on such a shared record does to the population that produced it; the guiding example is a tagged particle and the cage of z neighbors that drives its force history. Using a Girsanov path transformation, we prove that the conditioning multiplies the independent joint law of the z trajectories by exactly one term: a centered-square penalty along the single collective direction the record can see. Any fixed pair of particles stays nearly independent, with covariance falling as $O(z^{-1})$ and mutual information as $O(z^{-2})$, the property known as propagation of chaos, yet the $z(z-1)$ weak pair correlations add coherently into a finite suppression of collective fluctuations, the Schur shield $D - C = -C^2(aI + C)^{-1} \le 0$. The physical consequence is a calculable baseline for dynamical heterogeneity: conditioning itself contributes a computable, nonpositive amount to the susceptibility of a conditioned ensemble, so the genuine cooperative signal is the excess of a susceptibility measured at fixed record over this baseline rather than over zero. Finally, we provide a concrete protocol to test these predictions on trajectory data, and verify it on simulated trajectories of an exactly solvable Brownian model.

© 2026 Author(s). All article content, except where otherwise noted, is licensed under a Creative Commons Attribution-NonCommercial-NoDerivs 4.0 International (CC BY-NC-ND) license (https://creativecommons.org/licenses/by-nc-nd/4.0/). https://doi.org/10.1063/5.0355816

I. INTRODUCTION

When a liquid is cooled toward its glass transition, its average structure barely changes, but its dynamics breaks into bursts: compact groups of particles rearrange while nearby regions stay frozen.[1–4] How this cooperative motion emerges without static structural order or strong pair correlations remains a central problem in glass physics.

Experiments and simulations measure the cooperativity with dynamic propensities, four-point susceptibilities $\chi_4(t)$, and correlated displacement fields.[5–8] Each of these observables sums fluctuations over a large population, using collective coordinates computed from the very trajectories under study. Conditioning trajectories on a record they generated can produce a coherent population response even when the particles barely interact.

A tagged particle in a dense liquid is the guiding physical realization (Fig. 1): the record X is its measured trajectory, such as that of a tracer followed by confocal microscopy;[9,10] the z hidden paths are its caging neighbors; and the aggregate signal is the collective force the cage exerts on the tracer.

Because this record is generated by the particles it monitors, conditioning on it introduces an effective constraint: fixing X penalizes collective excursions that would alter the observed history, while history-to-history variations align particles through their shared response.

A separation of scales governs this conditioning. In an exchangeable population of size z (where particle labels can be permuted without changing the joint law), any fixed pair of particles becomes asymptotically independent with covariance $O(1/z)$ by propagation of chaos.[11–14] A bulk susceptibility, however, sums

© Author(s) 2026

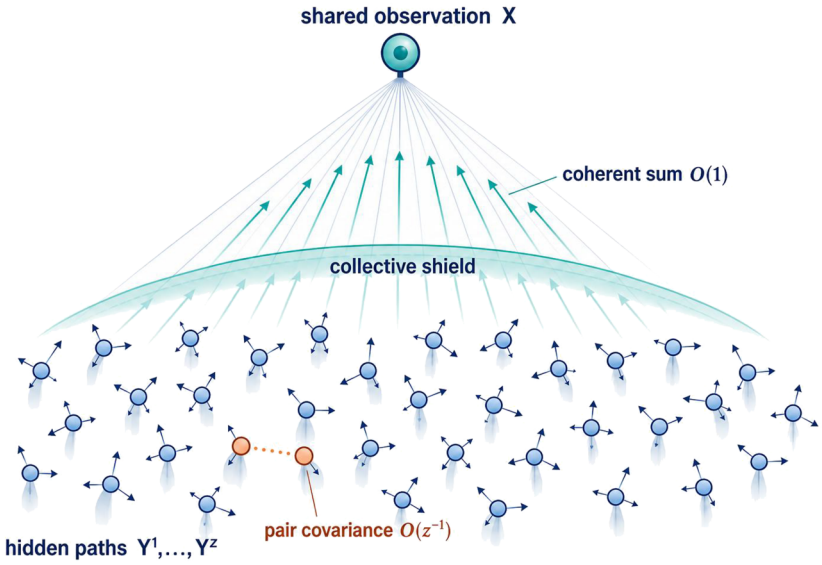


FIG. 1. Schematic of the conditioning geometry. A measured tracer trajectory X (top) is driven by the collective force of z caging neighbors $Y^1,\ldots,Y^z$. Conditioning on X compresses fluctuations along the visible collective direction (translucent shield) while leaving individual degrees of freedom nearly independent. Thin lines: individual path contributions; arrows: coherent sum; arc: the shield; orange: a tagged pair.

over all $z(z-1)$ pairs, so weak pair correlations accumulate into an $O(1)$ collective signal. Pair independence and collective heterogeneity therefore coexist; quantifying how much of this collective signal originates purely from the observation itself is critical to isolating genuine cooperative dynamics.

A. Physical origin and historical development

In glass physics, prior study has established that dynamical susceptibilities depend on whether conserved quantities[15] or initial configurations[6,7] are fixed; here we study conditioning on a different object: a noisy dynamical record generated by the monitored particles themselves. Two mathematical traditions frame the problem. One, running from Kac's and McKean's founding analyses of molecular chaos[16,17] to modern quantitative bounds,[12–14] proves that fixed pairs decouple, with covariance of order $1/z$. The other, developed by Ellis and Newman, Bolthausen, and Kusuoka and Liang, evaluates the fluctuations of population sums and shows that they stay finite.[18–20]

Mathematical work connects these two scales through conditional common noise and entropy bounds[12,21,22] but leaves open the explicit interaction produced when a population drives its own observation.

Here, we determine this interaction analytically. A Girsanov change of measure proves that conditioning on the record multiplies the independent path measure by a single centered-square penalty [Eq. (2)]. This penalty acts exclusively along the collective direction visible to the record, suppressing collective fluctuations through an operator inequality that we define as the Schur shield. Individual pairs maintain $O(1/z)$ covariance and $O(1/z^2)$ mutual information, while their coherent sum yields an $O(1)$ negative correction to the collective susceptibility. A quantitative sign threshold then separates this negative shield from the positive alignment generated by history-to-history variability, establishing a rigorous conditioning-only baseline for dynamical heterogeneity. Beyond propagation-of-chaos bounds on pairwise dependence, we derive the signed pair covariance with its leading prefactor and the closed-form conditioning-only shield, and we provide a simulation-tested trajectory-data protocol for estimating the shield and propensity variance separately.

B. Why the distinction matters

Separating true pairwise interactions from observation-induced shielding matters wherever collective observables are built from trajectories. In glassy liquids, four-point susceptibilities and dynamic propensities quantify spatial heterogeneity,[5–8,23,24] and time-domain optical spectroscopy follows the crossover from fast local motion to mode-coupling relaxation through one recorded collective signal.[25–28] The theorem gives all of them one controlled baseline: the exact conditioned component that any analysis built on a shared record contains.

The calculation also speaks to two established bodies of theory. Projection formalisms and mode-coupling hierarchies separate tagged particles or collective order parameters from their environment,[29–32] with modern versions retaining multi-point and multi-time correlators;[33–38] the theorem states exactly what conditioning on an aggregate output does to the remaining degrees of freedom, namely a rank-one penalty. Mathematical studies of pair decoupling[13,14,39,40] and of bulk fluctuations[18–20,41] treat the two scales separately; keeping the explicit $1/z$ pair covariance is what connects them.

The derivation rests on three core tools: (i) Girsanov path transformations between drift-shifted dynamics, (ii) Gaussian conditioning, under which inverse covariances add, and (iii) the law of total covariance. Table I (Appendix F) outlines all theoretical results, governing equations, proofs, and assumptions; Table II (Appendix G) summarizes the principal notation.

One conditional law yields the pair covariance prefactor, its $1/z^2$ information cost, and the resummed susceptibility, and it cleanly splits fluctuation suppression at fixed history from variance generated across histories. Section II derives the penalty and

© Author(s) 2026

TABLE I. Main theoretical results, corresponding equations, proofs, and underlying assumptions.

Result	Stated in	Proved in	Assumptions
Conditioning adds one centered-square penalty	Equation (2)	Appendix A	Bounded f; Lipschitz coefficients; fixed window $[0, T]$; $z^{-1/2}$ scaling; independent priors
Conditioned covariance $D = aC(aI + C)^{-1}$; Schur shield $D - C \preceq 0$	Equations (4) and (5)	Appendix C	As above; large z
Pair covariance $-(1/z)\langle b_u, (aI + C)^{-1} b_v\rangle$; mutual information $O(z^{-2})$	Equation (6)	Appendix B	Bounded single-particle observables
Fixed-history collective susceptibility $\chi_u^{(z)}$	Equation (8)	Appendix C	As above
Sign threshold	Equation (11)	Appendix D	exchangeability; law of total covariance
Closed-form dynamic Gaussian check	Equation (13)	Appendix E	Linear Gaussian model; stationary; full history observed

TABLE II. Summary of mathematical notation, physical interpretations, and first appearance.

Symbol	Physical/mathematical meaning	First used
z	Number of hidden particles driving the record (cage coordination number)	Section I
$X = (X_t)_{0\le t\le T}$; x	The record (measured trajectory on $[0, T]$); random path/one realization	Equation (1)
Y^i; y_i	Hidden path of particle i; random path/one realization	Equation (1)
$f(X_t, Y_t^i)$	Drift (force) that particle i exerts on the record; bounded	Equation (1)
σ_0, $a = \sigma_0^2$	Noise amplitude of the record and its variance per unit time (observation noise)	Equations (1) and (2)
$G_x(y)\ (t) = f(x_t, y_t)$	Drift contribution of one hidden path, as a function of $t \in [0, T]$	Equation (2)
$\langle g, h\rangle$, $\|g\|$	$\int_0^T g(t)h(t)\ \mathrm{d}t$ and the corresponding $L^2([0, T])$ norm	Equation (2)
Q_x; $Q_x^{\otimes z}$	One-path law given record ("tilted law"); z independent copies	Equation (2)
P_z^x	Exact joint law of z hidden paths conditioned on $X = x$	Equation (2)
$Z_z(x)$	Normalization constant (partition function)	Equation (2)
$m_x = \mathbb{E}_{Q_x} G_x$	Mean drift contribution of one path under tilted law	Equation (2)
$\widetilde{G}_i = G_x(Y^i) - m_x$	Centered drift contribution of particle i	Section II
$g \otimes g$	Tensor product operator $h \mapsto g\langle g, h\rangle$	Section II
C	Covariance operator of $\widetilde{G}_i$ under Q_x; kernel $C(t,s) = \mathbb{E}_{Q_x}[\widetilde{G}_i(t)\widetilde{G}_i(s)]$	Section II
$S_z = z^{-1/2}\sum_i \widetilde{G}_i$	Normalized collective drift fluctuation (the visible direction)	Equation (4)
D	Conditioned covariance operator of S_z in large-z limit	Equation (4)
$A \preceq B$	Loewner partial order: $B - A$ is positive semidefinite	Equation (5)
c	Eigenvalue of C (variance of one collective visible mode)	Section II
u, v; $u_i = u(Y^i)$	Bounded single-particle observables (displacement, cage overlap, etc.)	Equation (6)
$b_u(t) = \mathrm{Cov}_{Q_x}(u(Y), G_x(Y)(t))$	Coupling of observable u to the visible force direction at time t	Equation (6)
$\chi_u^{(z)}$	Variance of normalized collective observable $z^{-1/2}\sum_i u_i$ at fixed history	Equation (8)
$\mu_z(X) = \mathbb{E}[u(Y^1) \mid X]$	Dynamic propensity given history X	Section IV
$h_z(X) = \sqrt{z}\,[\mu_z(X) - \mathbb{E}\mu_z(X)]$	Normalized propensity fluctuation on collective scale	Section IV
v_X, δ_X	Single-path conditional variance $\mathrm{Var}(u(Y^1) \mid X)$; Schur shield for history X	Equations (9) and (10)
ξ	Alignment: Correlation coefficient between $u(Y)$ and the force its particle exerts on the record; $\xi = \lvert b_u\rvert/\sqrt{\mathrm{Var}\,(u)\ c}$	Figure 2
$\lambda, \sigma^2, g, k_0, D_0, \alpha$	Parameters of solvable Gaussian process (k_0 is the relaxation rate of the record)	Section V

© Author(s) 2026

the shield. Section III computes the pair covariance and resums it. Section IV allows the record to fluctuate and derives the sign threshold. Section V evaluates everything exactly in a solvable dynamical model, Sec. VI provides a step-by-step measurement protocol (Sec. VI A) with its calibration and a numerical test (Sec. VI B), and Sec. VII concludes.

II. A FINITE-POPULATION PATH MODEL

Consider z hidden trajectories driving a noisy aggregate path. Fixing this path penalizes collective deviations that would alter the record, creating correlations restricted to the collective mode visible to the measurement.

Let $Y^1, \ldots, Y^z$ denote hidden stochastic paths, and let X denote an aggregate output driven by their collective drift

$$\mathrm{d}X_t = b_0(X_t)\,\mathrm{d}t + \frac{1}{\sqrt{z}}\sum_{i=1}^{z} f(X_t, Y_t^i)\,\mathrm{d}t + \sigma_0\,\mathrm{d}B_t, \tag{1}$$

on $[0,T]$, with bounded f and Lipschitz coefficients. The coupled dynamics in which the hidden particles drive the record, Eq. (1), is the endogenous dynamics. For a tagged tracer, X_t is the tracer position, b_0 is its bare drift, $f(X_t, Y_t^i)$ is the force from neighbor i, and $\sigma_0\,\mathrm{d}B_t$ is the tracer's thermal noise. Under a reference dynamics without collective drift, $\mathrm{d}X_t = b_0(X_t)\,\mathrm{d}t + \sigma_0\,\mathrm{d}B_t$, the hidden paths are mutually independent given $X = x$. Girsanov's theorem[42,43] gives the Radon–Nikodym derivative (reweighting factor) between the two measures. The $z^{-1/2}$ normalization keeps the collective force comparable to the output noise as $z \to \infty$.

The derivation has three steps (details in Appendix A). First, Girsanov's theorem gives the weight of the endogenous dynamics relative to the reference dynamics as the exponential of a term linear in the collective force $F_z(t) = z^{-1/2}\sum_i f(X_t, Y_t^i)$ and a term quadratic in it, $-(2a)^{-1}\int_0^T F_z(t)^2\,\mathrm{d}t$. Second, the linear term is a sum over particles, so it reweights each path separately and couples nothing; only the quadratic term, $-(2az)^{-1}\|\sum_i G_x(y_i)\|^2$, contains products of different particles. Third, completing the square about the one-path mean m_x splits off further single-particle terms, which are absorbed into the one-path law Q_x, and constants, which are absorbed into the normalization $Z_z(x)$. What remains is the conditional posterior in the closed form

$$\frac{\mathrm{d}P_z^x}{\mathrm{d}Q_x^{\otimes z}}(y_1, \ldots, y_z) = \frac{1}{Z_z(x)}\exp\left[-\frac{1}{2az}\left\|\sum_{i=1}^{z}\left(G_x(y_i) - m_x\right)\right\|^2\right]. \tag{2}$$

Here, P_z^x is the exact joint law of the z hidden paths conditioned on $X = x$, while $Q_x^{\otimes z}$ denotes the product measure of z independent copies under the one-path tilted law Q_x (the single-path distribution reweighted by its interaction with the record). The function $G_x(y)\ \ (t) = f(x_t, y_t)$ is the drift contribution of a single path, $m_x = \mathbb{E}_{Q_x} G_x$ is its mean, $a = \sigma_0^2$ is the output-noise variance, and $Z_z(x)$ is the normalization. The inner product and norm are those of $L^2([0,T])$, $\langle g, h\rangle = \int_0^T g(t)h(t)\,\mathrm{d}t$ and $\|g\|^2 = \langle g, g\rangle$. As illustrated in Fig. 1, conditioning penalizes only the coherent sum of the path contributions along the visible direction, leaving any tagged pair with only an $O(z^{-1})$ constraint. Every one-body effect is absorbed into Q_x. The entire many-body interaction is the single centered square. All remainders quoted below are nonasymptotic and dimension free at this fixed window, with constants depending only on the force bound, the window, and a; they are not uniform on a window that grows with the relaxation time (Sec. V).

Each object in Eq. (2) has a direct physical reading. The law Q_x describes one hidden path responding to the recorded history. The function G_x converts that path into its predicted contribution to the record. The centered sum measures how far the population would push the output away from the value already conditioned on, and a sets the tolerance: a noisy output forgives collective deviations and a precise output penalizes them. The minus sign expresses a constraint, not a force. The population cannot collectively move a signal that has already been fixed.

The interaction is rank structured: the z paths interact exclusively through the single collective variable $\sum_i[G_x(y_i) - m_x]$ (the visible direction), whereas a general pair interaction would require $O(z^2)$ independent couplings. Microscopic motion that leaves G_x unchanged still follows the independent one-path law to leading order; only the visible direction is screened. This predicts anisotropic suppression: two observables with the same single-particle variance can pick up very different collective corrections depending on how strongly they overlap with the measured output. The representation holds on a separable Hilbert space, so time-dependent observation needs no discretization of the path.

Define the centered observation variable $\widetilde{G}_i = G_x(Y^i) - m_x$ under Q_x, with covariance operator,

$$C = \mathbb{E}_{Q_x}[\widetilde{G}_i \otimes \widetilde{G}_i]. \tag{3}$$

For the normalized sum $S_z = z^{-1/2}\sum_i \widetilde{G}_i$, the conditional covariance has the large-z limit,

$$\mathrm{Cov}_{P_z^x}(S_z) = D + O(z^{-1}), \qquad D = aC(aI + C)^{-1}. \tag{4}$$

Equation (4) follows from Gaussian conditioning: for large z, the central limit theorem makes S_z Gaussian with covariance C under the independent law, while the penalty in Eq. (2), $\exp(-\|S_z\|^2/2a)$, acts as a conjugate Gaussian factor with covariance aI. Combining these two factors adds their inverse covariances, $D^{-1} = C^{-1} + a^{-1}I$, yielding Eq. (4) (Appendix C).

Since

$$D - C = -C^2(aI + C)^{-1} \le 0, \tag{5}$$

the observation reduces the visible collective fluctuations in every direction. We call this operator difference the Schur shield. Here, $A \le B$ means that $B - A$ is positive semidefinite, i.e., $\langle\phi, A\phi\rangle \le \langle\phi, B\phi\rangle$ for every $\phi \in L^2([0,T])$: conditioning does not increase the variance of the collective drift along any direction ϕ. The name refers to the Schur complement, the matrix identity that gives the covariance of a Gaussian vector after conditioning on a noisy linear observation.

Diagonalizing C makes the shield concrete. An eigenmode of variance c ends up with conditioned variance $ac/(a + c)$: weakly observed modes with $c \ll a$ barely change, while strongly visible modes with $c \gg a$ saturate at the observation-noise scale. This is the rule that combines two resistors in parallel, applied mode by mode. It also shows that the shield can never overshoot: it subtracts a positive component while the total response stays positive. Figure 2(a)

© Author(s) 2026

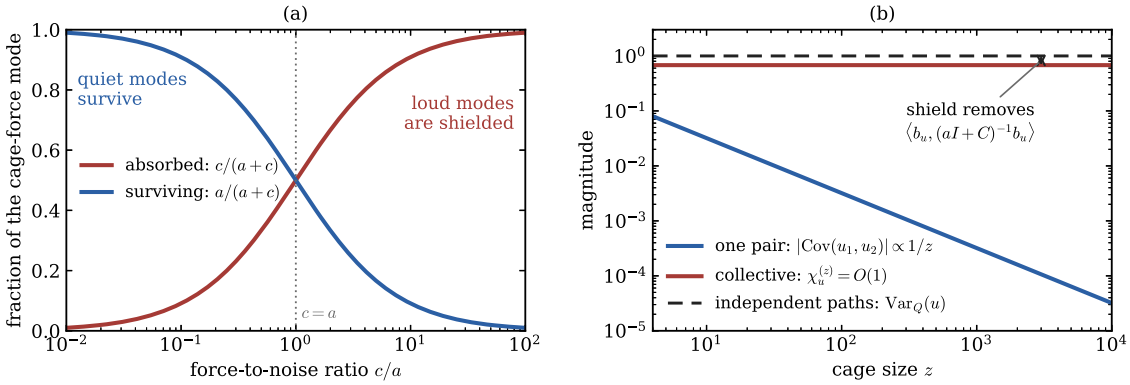


FIG. 2. Shared output selectively absorbs collective motion. (a) An eigenmode of one-path variance c splits into an absorbed share $c/(a+c)$ and a surviving share $a/(a+c)$ as its force-to-noise ratio c/a grows. (b) At fixed history, a tagged pair decorrelates as $1/z$ with the cage size z, the number of neighbors driving the record, while the normalized population sum retains the order-one shield $\langle b_u, (aI+C)^{-1}b_u\rangle$. The dashed line shows the value for independent paths, $\mathrm{Var}_{Q_x}(u)$. The curves plot the analytical predictions of Eqs. (4)–(6) and (8). Panel (b) uses $\mathrm{Var}(u) = 1$, $c/a = 1$, and $\xi = 0.8$ (the alignment defined in Sec. IV), as in Fig. 4.

plots the two shares against the force-to-noise ratio c/a: the surviving share $a/(a+c)$ and the absorbed share $c/(a+c)$ cross at $c = a$.

III. PAIR INDEPENDENCE WITH A COLLECTIVE CORRECTION

Local observables and collective observables scale differently with population size z. Fixed pairs decorrelate as $z \to \infty$, yielding asymptotic independence. Summing weak cross-correlations across all $z(z-1)$ pairs, however, yields a finite collective response. We analyze both limits directly: integrating out all but two tagged paths yields the leading-order pair covariance, which is then resummed across the population.

Removing two labels and integrating over the other $z-2$ paths leaves a two-body log density of order $1/z$ with a centered leading term. The operator $(aI+C)^{-1}$ arises from screening: the cross term of the square in Eq. (2) gives the bare coupling $-(az)^{-1}\langle \widetilde{G}_1, \widetilde{G}_2\rangle$ between two labels, while the remaining $z-2$ paths partially screen this interaction, replacing a^{-1} with $a^{-1} - a^{-2}D = (aI+C)^{-1}$ (Appendix B). For bounded single-particle observables u and v,

$$\mathrm{Cov}_{P_z^x}\big(u(Y^1), v(Y^2)\big) = -\frac{1}{z}\big\langle b_u, (aI+C)^{-1} b_v\big\rangle + O(z^{-3/2}), \qquad (6)$$

where

$$b_u = \mathrm{Cov}_{Q_x}(u(Y), G_x(Y)), \qquad (7)$$

where b_u is a function of time on $[0,T]$: $b_u(t)$ is the covariance between the observable and the force that the same particle exerts on the record at time t. An observable uncorrelated with that force has $b_u = 0$ and is not affected by the conditioning. For $u = v$, the bracket in Eq. (6) is non-negative, so the covariance is nonpositive and negative whenever $b_u \neq 0$: given the record, a larger contribution from one particle must be compensated by the others.

The pair mutual information is smaller, of order $1/z^2$, because relative entropy starts at the quadratic term in the small centered density perturbation: for a density of the form $1 + \epsilon\,\psi$ with ψ centered, covariances scale as ϵ while mutual information scales as ϵ^2; here $\epsilon = 1/z$.

Covariance and mutual information decay at different rates for the same pair. A signed observable responds linearly to the $1/z$ density perturbation, whereas mutual information discards the sign and begins quadratically. Consequently, a small pair mutual information does not bound the summed collective susceptibility; the physically relevant quantity is the pair covariance projected onto the visible direction.

Summing across all pairs yields the collective susceptibility. For the normalized population observable $z^{-1/2}\sum_i u(Y^i)$, the fixed-history susceptibility $\chi_u^{(z)} \equiv \mathrm{Var}_{P_z^x}\big(z^{-1/2}\sum_i u(Y^i)\big)$ resums from Eq. (6) to

$$\chi_u^{(z)} = \mathrm{Var}_{Q_x}(u) - \big\langle b_u, (aI+C)^{-1} b_u\big\rangle + O(z^{-1/2}). \qquad (8)$$

The second term is nonpositive, and it contains no adjustable parameter once the one-path law is known. Equations (6) and (8) hold simultaneously: local and collective observables probe different sums of the same weak correlation field. Figure 2(b) illustrates both statements: the pair covariance falls as $1/z$ (blue), while the collective variance stays a fixed distance, the shield, below its independent-path value, $\mathrm{Var}_{Q_x}(u)$ (red and dashed).

In the variance of $z^{-1/2}\sum_i u(Y^i)$, the z diagonal terms yield the single-particle variance, while the $z(z-1)$ off-diagonal pairs each contribute $O(1/z)$; after the $1/z$ normalization, their sum is an order-one correction. Consequently, pair independence for fixed labels does not imply collective independence in the double sum.

IV. FLUCTUATING HISTORIES AND DYNAMICAL HETEROGENEITY

A history is one realization of the record; "fixed history" and "fixed record" are used interchangeably. When observed histories vary across experimental runs, each history shifts the conditional mean of a tagged observable, $\mu_z(X) = \mathbb{E}[u(Y^1) \mid X]$ (the propensity). With $u_i = u(Y^i)$, these identical shifts add coherently in the

© Author(s) 2026

normalized collective observable $\widetilde{U}_z = z^{-1/2}\sum_i [u_i - \mathbb{E}u]$: exchangeability gives $\mathbb{E}[\widetilde{U}_z \mid X] = \sqrt{z}\,[\mu_z(X) - \mathbb{E}\mu_z(X)] \equiv h_z(X)$. The factor $\sqrt{z}$ amplifies single-particle propensity fluctuations of order $z^{-1/2}$ into an $O(1)$ collective variation. This order holds when the feedback of the record on each hidden path is weak, of order $z^{-1/2}$, as Newton's third law gives for the scaled coupling of Eq. (1); with $O(1)$ feedback, which Appendix A also allows, $\mathrm{Var}(h_z)$ is of order z. Let v_X be the single-path conditional variance and let

$$\delta_X = \left\langle b_X, (aI + C_X)^{-1} b_X \right\rangle \geq 0, \tag{9}$$

be the Schur shield for that history, where b_X and C_X denote b_u and C evaluated for the history X. The law of total variance gives

$$\mathrm{Var}\,(\widetilde{U}_z) = \mathbb{E}[v_X - \delta_X] + \mathrm{Var}\,(h_z(X)) + O(z^{-1/2}). \tag{10}$$

For two different labels,

$$z\,\mathrm{Cov}\,(u_1, u_2) = \mathrm{Var}\,(h_z(X)) - \mathbb{E}\delta_X + O(z^{-1/2}). \tag{11}$$

Equation (11) is the law of total covariance, $\mathrm{Cov}\,(u_1, u_2) = \mathbb{E}[\mathrm{Cov}\,(u_1, u_2 \mid X)] + \mathrm{Cov}\,(\mathbb{E}[u_1 \mid X], \mathbb{E}[u_2 \mid X])$, with Eq. (6) inserted in the first term and $\mathbb{E}[u_1 \mid X] = \mathbb{E}[u_2 \mid X] = \mu_z(X)$ in the second.

Equation (11) sets up a competition between two effects of opposite sign: a shared fixed observation suppresses redundant collective motion, whereas variation between observed histories aligns particles through a common propensity. The measured cross-correlation changes sign when the propensity variance overtakes the mean shield. This defines the conditioned-population susceptibility, supplying the controlled component that matches a chosen experimental ensemble. Figure 3 plots Eq. (11) for a single visible mode. Each line has a unit slope and intercept $-\mathbb{E}\delta_X = -\xi^2\mathrm{Var}\,(u)\,c/(a+c)$, where the alignment $\xi \in [0,1]$ is the magnitude of the correlation coefficient between the observable and the force its particle exerts on the record. The dot on each line marks the threshold $\mathrm{Var}\,(h_z) = \mathbb{E}\delta_X$ at which the cross-particle covariance changes sign.

This decomposition explains why dynamical susceptibilities depend sensitively on the conditioning protocol.[15] Two analyses can report opposite cross-particle signs for identical microscopic dynamics by conditioning on different information: fixing the macroscopic history isolates the negative shield, whereas averaging over histories adds the positive propensity variance. Reporting the two terms of Eq. (11) separately resolves this ambiguity and translates data between protocols.

The propensity defined here provides the path-space analog of the isoconfigurational propensity.[6,7,44] The present result establishes the sign and the closed-form expression of the fixed-record contribution when the conditioning variable is a noisy aggregate record. For a two-time cage overlap, $\mu_z(X)$ is a conditional mobility propensity, with the observed history playing the role of the fixed initial configuration in the isoconfigurational ensemble.[6,8] Equation (11) then establishes a quantitative threshold: history-to-history propensity fluctuations must exceed the force-aligned shield before cross-particle dynamical heterogeneity turns positive. Repeated runs from stored configurations, or any other conditional ensemble, can locate this threshold, while the testable physical content is the predicted value of the shield (Step 4 of Sec. VI A).

Equation (11) dictates how to interpret both conditioned and unconditioned measurements (Fig. 4). The physical meaning of the

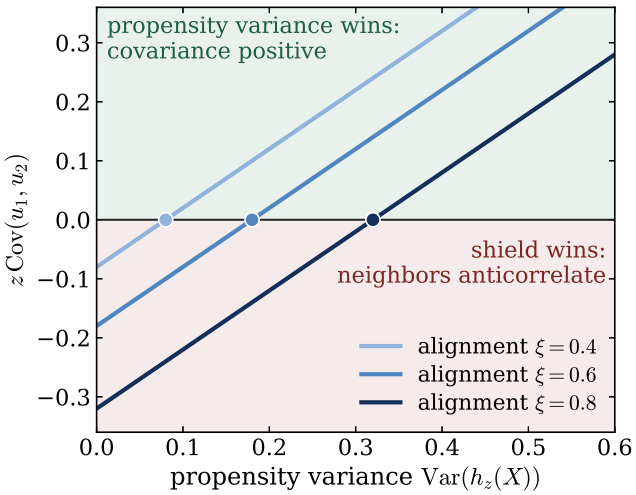


FIG. 3. Two sources set the sign of the cross-particle response. Each line is Eq. (11) for one alignment ξ: unit slope, intercept $-\mathbb{E}\delta_X$. Below zero (red), the shield wins and neighbors anticorrelate; above zero (green), the propensity variance wins. The dots mark the sign change. The curves are labeled by the alignment $\xi \in [0,1]$, the correlation coefficient between the observable and the force its particle exerts on the record, for which the scalar shield is $\mathbb{E}\delta_X = \xi^2\mathrm{Var}\,(u)\,c/(a+c)$. The crossing implements Eq. (11) without an adjustable sign convention.

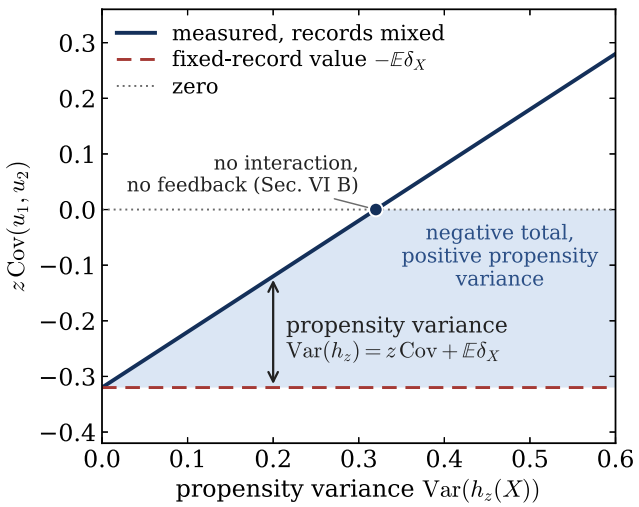


FIG. 4. Reading a susceptibility against the baseline. At fixed record, the non-interacting null is the negative baseline $-\mathbb{E}\delta_X$ (dashed), not zero (dotted); a measurement above $-\mathbb{E}\delta_X$ indicates positive within-record correlation. In an unconditioned ensemble, zero is the independent null, but the baseline $-\mathbb{E}\delta_X$ identifies the hidden propensity variance $\mathrm{Var}\,(h_z) = z\,\mathrm{Cov}\,(u_1, u_2) + \mathbb{E}\delta_X$ (arrow) masked by cancellation with the shield. In the shaded band, the net covariance is negative, yet particles share a positive propensity variance that comparison with zero would miss. Parameters as in Figs. 2 and 3: $\mathrm{Var}(u) = 1$, $c/a = 1$, $\xi = 0.8$, so $\mathbb{E}\delta_X = 0.32$. The dot marks particles that neither interact with nor feel the record, for which the two terms cancel exactly (Sec. VI B).

© Author(s) 2026

baseline depends on the ensemble being analyzed: (i) Within a fixed record (conditioned ensemble), the true null hypothesis for non-interacting particles is not zero but the negative baseline $-\delta_X$ ($-\mathbb{E}\delta_X$ on average). Conditioning on the shared record penalizes redundant collective motion and forces an apparent anticorrelation of order $1/z$; any measured $z\,\mathrm{Cov}(u_1, u_2 \mid X)$ exceeding $-\delta_X$ indicates positive within-history coordination. (ii) Across records (unconditioned or mixed-history ensemble), the null hypothesis for independent non-interacting particles is identically zero. Here, $-\mathbb{E}\delta_X$ serves as an accounting baseline rather than an independence threshold: an unconditioned covariance near zero does not imply dynamically inert particles, but can reflect an exact cancellation between the negative shield $-\mathbb{E}\delta_X$ and an equally large positive propensity variance $\mathrm{Var}(h_z(X))$, as shown explicitly in Sec. VI B. The excess over $-\mathbb{E}\delta_X$ isolates the total propensity variance that particles acquire by following a shared record. Comparing an unconditioned susceptibility directly with zero underestimates the propensity variance by exactly the shield magnitude.

Ensemble and response analyses of dynamic fluctuations ask how a bulk liquid builds a growing correlated volume.[15,45–47] Equation (11) identifies one contribution that the observation protocol itself adds or removes, and it tells the experimentalist exactly which two numbers to report: the fixed-history shield and the between-history propensity variance.

V. DYNAMIC GAUSSIAN CALIBRATION

The operator formulas distinguish visibility at an instant from visibility accumulated over a history. A solvable Gaussian process checks that this distinction is dynamical rather than notational: the same observation constraint passes through two relaxation filters, and the equal-time and time-integrated responses come out different.

The model makes every symbol concrete. On the whole timeline, let the hidden coordinates be independent stationary Ornstein–Uhlenbeck processes, and let the record integrate their collective pull

$$\begin{aligned} \mathrm{d}y_i &= -\lambda y_i\,\mathrm{d}t + \sqrt{2\lambda\sigma^2}\,\mathrm{d}W_i, \\ \mathrm{d}x &= \left[-k_0 x + \frac{g}{\sqrt{z}}\sum_{i=1}^{z} y_i\right]\mathrm{d}t + \sqrt{2D_0}\,\mathrm{d}W_0, \end{aligned} \tag{12}$$

with independent Brownian motions, rates $k_0, \lambda > 0$, coupling g, hidden stationary variance σ^2, and output-noise intensity D_0. Conditioning on the complete stationary x history is a classical Gaussian smoothing problem,[48] so the posterior is Gaussian and every operator can be evaluated exactly (Appendix E). Comparing Eq. (12) with Eq. (1) gives $f(x, y) = g\,y$ and $\sigma_0^2 = 2D_0$ so that $G_x(y)\ (t) = g\,y(t)$ and $a = 2D_0$. (In Appendix E it is convenient to divide the record by g, which gives the equivalent pair $a = 2D_0/g^2$ with $C(\omega)$ the spectrum of y itself.) The model is solved exactly and independently of the general theorem (Appendix E). It reproduces the formulas of Secs. II–IV with an unbounded linear force, which shows that the structure of the result does not hinge on the boundedness assumption. The cross-covariance of two hidden paths takes the form

$$\begin{aligned} \mathrm{Cov}\left[y_i(t), y_j(s) \mid x\right] &= -\frac{\sigma^2}{z}\left[e^{-\lambda|t-s|} - \frac{\lambda}{\alpha}e^{-\alpha|t-s|}\right], \\ \alpha^2 &= \lambda^2 + \frac{g^2\lambda\sigma^2}{D_0}. \end{aligned} \tag{13}$$

The formula confirms the $1/z$ pair scale and the negative sign at fixed history, and it separates the two responses: the predictable fraction, defined as the share of collective variance removed by the record, $1 - D/C$, equals $1 - \lambda/\alpha$ at equal times and $1 - \lambda^2/\alpha^2$ for time-integrated observables (zero frequency). No single static coupling reproduces both numbers: a reduced model replacing the path-space operator $(aI + C)^{-1}$ with a scalar cannot match the two. Temporal filtering is part of the physical susceptibility.

The two rates admit direct physical interpretations: λ represents the intrinsic relaxation rate of a single hidden coordinate, while α incorporates the precision and coupling strength of the aggregate observation. The anticorrelation decays at the slower rate λ, while α sets its short-time rounding. Equal-time measurements sample the instantaneous overlap of the two filters, the time-integrated response weights their lifetimes, and the comparison distinguishes a genuinely dynamical shield from a static covariance constraint.

The theorem is uniform on every fixed observation window $[0, T]$. Extending it to windows that grow with the structural relaxation time requires a bound on how fast the hidden paths lose memory (a mixing or dissipativity estimate) to control the error constants as $T \to \infty$.

VI. IMPLICATIONS

Conditioning on a shared record applies no physical forces to the particles; the underlying microscopic dynamics remains unchanged. What changes is the statistical ensemble: among all possible realizations, only trajectories consistent with the record are retained, and Eq. (2) determines their exact reweighting. Raising the observation precision suppresses fluctuations along the visible direction through $(aI + C)^{-1}$ while leaving orthogonal modes unaffected. This identifies two independently tunable experimental parameters: observation precision and history diversity.

The result also refutes an inference commonly drawn from local measurements. Pair mutual information of order $1/z^2$ does not bound the collective response, because $z(z-1)$ weak signed correlations aligned along one direction survive the sum. Wherever an aggregate record is driven by the constituents that produce it, including probe trajectories in crowded media,[49] coarse-grained order parameters, neural population recordings, and latent-variable models,[50] varying the measurement noise gives a direct experimental handle: visible susceptibilities scale with the shield factor, orthogonal ones do not.

A. A step-by-step protocol

The predictions involve only conditional means and covariances, so they can be estimated from trajectory data. The data required are N_h records $X^{(h)}$ and, for each record, N_r independent samples (replicas) of the z hidden paths consistent with it; $u_i^{(h,r)}$ denotes the chosen observable of particle i in replica r of record h. One run is a complete realization: the record together with all z hidden paths. With ordinary independent simulations, each of the

© Author(s) 2026

N runs has its own record; sort runs by the Step 1 summary $\phi(X)$ into N_h equal-occupancy bins, treat each bin as a record group with $N_r \approx N/N_h$ runs as replicas, and increase N_h until the summary-conditioned shield estimate $\hat{\delta}$ [Eq. (17)] reaches a plateau [Fig. 5(c): 10^5 runs, $N_h = 1, 2, 4, \ldots, 256$].

Step 0: Choose the record, the population, and the observable. In the tagged-particle example, the record is the tracer path on $[0, T]$, the population is its z nearest neighbors at time 0, and u is a bounded single-particle quantity such as a displacement component along the tracer–neighbor axis or a cage-overlap indicator.

Step 1: Group the data by record. Replicas must be drawn from the conditional distribution given the record X; in linear Gaussian models, they can be generated directly by conditioned Gaussian simulation, whereas general models require Girsanov reweighting or grouping runs that share the record summary. With stored trajectories where the record cannot be held fixed exactly, runs are grouped by a summary $\phi(X)$ of the path: bins of a scalar summary, or the prediction of a regression of the observable on the sampled record. Any such grouping conditions on less than the full path, and the law of total covariance gives $z\,\mathbb{E}[\mathrm{Cov}\,(u_1, u_2 \mid \phi)] = -\mathbb{E}\delta_X + \mathbb{E}[\mathrm{Var}\,(h_z \mid \phi)]$. The estimate is therefore less negative than the full-path value, never more, and for a coarse summary it can even be positive. Refining the bins removes only the part of the excess that is due to the bin width; the rest is set by how informative the summary is [Fig. 5(c)]. The summary should be chosen to maximize the shield estimate, and tests (i) and (iii) of Step 4 refer to that maximum. A regression predictor must be fitted on runs other than those it is used to group.

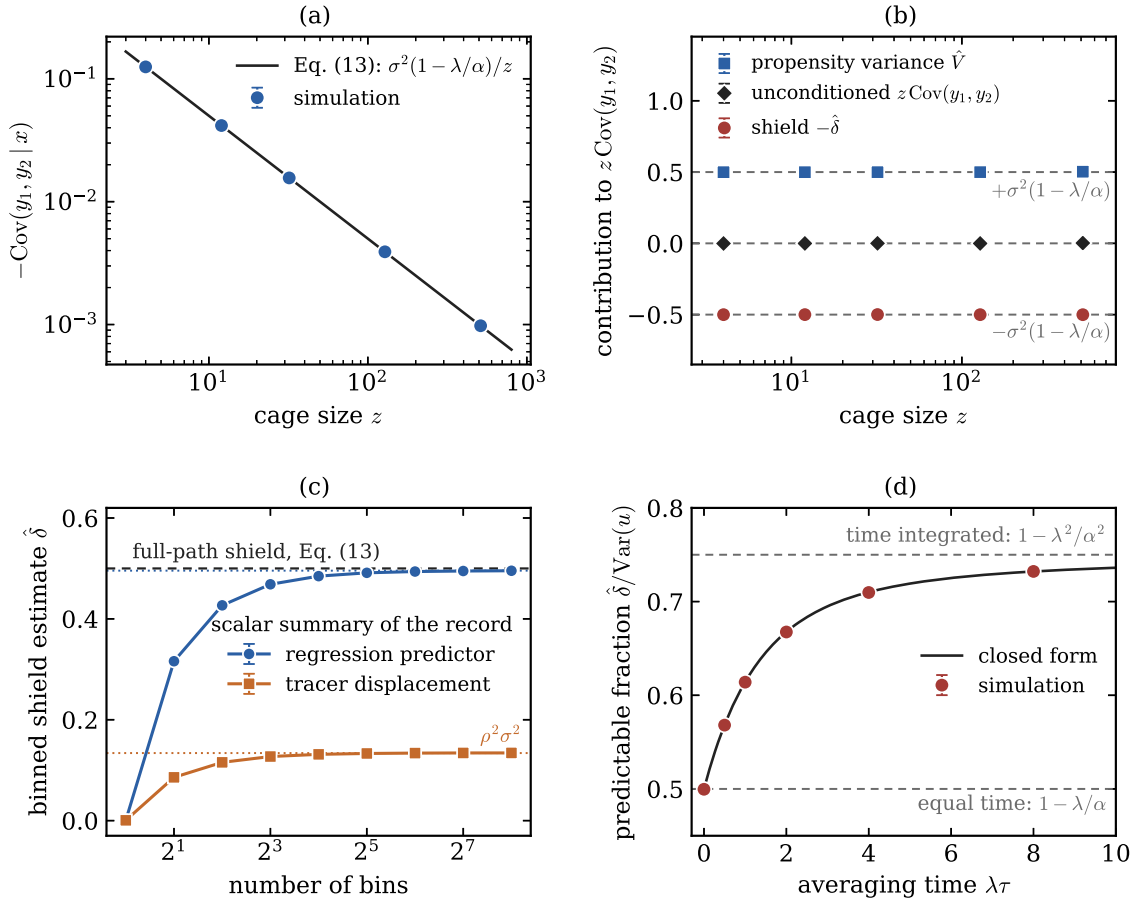


FIG. 5. Protocol of Sec. VI A applied to trajectories simulated from the solvable model, Eq. (12), with $\lambda = \sigma^2 = g = k_0 = 1$ and $D_0 = 1/3$ so that $\alpha = 2\lambda$; 10^5 runs per point, and the standard errors over 16 repeats are smaller than the symbols. No result of the theory enters the estimators. (a) Fixed-record pair covariance of $u_i = y_i(t)$, the record being fixed by linear regression on its increments, compared with Eq. (13). (b) Shield, propensity variance, and unconditioned covariance: the two terms are equal and opposite, and their sum vanishes because the hidden coordinates do not interact. (c) Steps 1–3 with the runs binned by a scalar summary of the record, $z = 12$. As the bins are refined, the estimate rises to $\rho^2\sigma^2$, where ρ is the correlation of the summary with the collective coordinate: an informative summary (the regression predictor, fitted out of sample) recovers 99% of the full shield, whereas the tracer displacement over one relaxation time recovers about a quarter of it. (d) Step 5: Predictable fraction of a time-averaged observable against the averaging time; the closed form interpolates between $1 - \lambda/\alpha$ and $1 - \lambda^2/\alpha^2$.

© Author(s) 2026

Step 2: Fixed-record pair covariance (the shield). For each record, compute the replica means and their average, the raw pair covariance, and the fixed-record collective variance,

$$\bar{u}^{(h,r)} = \frac{1}{z}\sum_i u_i^{(h,r)}, \qquad \hat{\mu}^{(h)} = \frac{1}{N_r}\sum_r \bar{u}^{(h,r)}, \tag{14}$$

$$\hat{c}^{(h)} = \frac{1}{N_r z(z-1)}\sum_r \sum_{i\neq j}\left(u_i^{(h,r)} - \hat{\mu}^{(h)}\right)\left(u_j^{(h,r)} - \hat{\mu}^{(h)}\right), \tag{15}$$

$$\hat{\chi}^{(h)} = \frac{z}{N_r - 1}\sum_r \left(\bar{u}^{(h,r)} - \hat{\mu}^{(h)}\right)^2. \tag{16}$$

Because $\hat{\mu}^{(h)}$ is estimated from the same replicas, $\hat{c}^{(h)}$ lies below the true pair covariance by $\chi^{(h)}/(zN_r)$ on average, where $\chi^{(h)} = \mathbb{E}\hat{\chi}^{(h)}$ is the true fixed-record collective variance. The shield estimate that removes this bias is

$$\hat{\delta} = -z\,\overline{\hat{c}^{(h)}} - \frac{\overline{\hat{\chi}^{(h)}}}{N_r}, \tag{17}$$

with the bars denoting averages over the N_h records; at least two replicas per record are required.

Step 3: Propensity variance. Compute

$$\hat{V} = z\,\mathrm{Var}_h\left(\hat{\mu}^{(h)}\right) - \frac{\overline{\hat{\chi}^{(h)}}}{N_r}, \tag{18}$$

where Var_h is the variance over records. The same term removes the sampling noise of $\hat{\mu}^{(h)}$ from both estimates. When every record has the same N_r and Var_h is normalized by N_h, $\hat{V} - \hat{\delta}$ reproduces the pooled sample value of $z\,\mathrm{Cov}(u_1, u_2)$ exactly.

Step 4: Report and test. Report $\hat{\delta}$ and $\hat{V}$ separately, together with the unconditioned $z\,\mathrm{Cov}(u_1, u_2)$. Their relation, the law of total covariance underlying Eq. (11), is an identity; it checks the estimators, not the theory. The tests of the theory are (i) the fixed-record covariance of a force-coupled observable is negative; (ii) it scales as $1/z$ at fixed shield; (iii) its magnitude is parameter free: b_u and C are single-particle covariances measurable from the same data and a is the noise variance of the record, so $\langle b_u, (aI + C)^{-1} b_u\rangle$ can be computed independently and compared with $\hat{\delta}$; (iv) it is selective: an observable with $b_u = 0$ shows no shield; and (v) it depends on the record noise through $c/(a + c)$ [Fig. 2(a)].

Step 5: Time-averaged observables and predictable fraction. Repeat with two temporal filters, equal-time and time-averaged. The difference between the two measures the path-space character seen in Eq. (13) [Fig. 5(d)].

B. Worked example: The solvable model

In the model of Sec. V, every quantity in the protocol is known in closed form. Take $u_i = y_i(t)$. Step 2 gives, from Eq. (13) at $t = s$, $\mathbb{E}\delta_X = \sigma^2(1 - \lambda/\alpha)$. The hidden coordinates of this model do not interact and are not influenced by the record, so their unconditioned covariance vanishes identically, and Eq. (11) then requires $\mathrm{Var}(h_z) = \sigma^2(1 - \lambda/\alpha)$; this can be confirmed directly from $\mathrm{Var}\,(y_i) = \mathbb{E}\mathrm{Var}\,(y_i \mid x) + \mathrm{Var}\,(\mu_z)$. The measured cross-covariance, zero, is thus the exact cancellation of two nonzero terms. For $g^2\sigma^2/(\lambda D_0) = 3$, one has $\alpha = 2\lambda$: the predictable fraction is $1 - \lambda/\alpha = 1/2$ at equal times (where the shield and propensity variance each equal $\sigma^2/2$), and $1 - \lambda^2/\alpha^2 = 3/4$ at zero frequency, where the shield absorbs three quarters of the unconditioned spectral density $C(0) = 2\sigma^2/\lambda$.

Figure 5 tests the protocol on $M = 10^5$ runs of Eq. (12) (Euler–Maruyama, $\Delta t = 0.005$, $T = 16$, $t^* = 8$), with the record sampled at an interval of 0.04 (400 increments ΔX_k). In Gaussian dynamics, linear regression of $\bar{u}$ on ΔX yields exact conditional expectations and residual variances without theoretical input. The fixed-record pair covariance follows $-\sigma^2(1 - \lambda/\alpha)/z$ over two decades in z [Fig. 5(a)]. The shield and propensity variance agree with exact formulas within one percent and cancel in the unconditioned covariance [Fig. 5(b)], while the predictable fraction of a time-averaged observable crosses over from $1 - \lambda/\alpha$ to $1 - \lambda^2/\alpha^2$ [Fig. 5(d)]. Figure 5(c) shows the effect of grouping by record summary (Step 1).

This benchmark establishes the physical meaning: non-interacting particles exhibit equal and opposite propensity variance and shield, so only their signed sum $\mathrm{Var}\,(h_z) - \mathbb{E}\delta_X$ is independent of conditioning. A nonzero sum signals coupling beyond the shared record, such as feedback (the X dependence in Appendix A) or direct interactions.

C. Scope of the test in molecular simulations

Applying the protocol to simulated liquids involves four practical considerations. First, the theorem applies directly to overdamped Langevin (Brownian) dynamics, where the tracer equation carries thermal noise with known variance $a = 2k_BT/\gamma$; Newtonian or underdamped dynamics require specifying an observation channel with defined noise. Second, for a first coordination shell ($z \approx 12$), finite-size corrections of order $z^{-1/2}$ affect the magnitude of the shield but not its sign or its mode selectivity. In dense liquids, direct pair interactions add their own covariance, so the measured fixed-record covariance need not be negative; the non-interacting shield δ_X computed via Step 4(iii) is the reference from which the direct contribution is read. Third, because coordination number z is fixed by local packing, $1/z$ scaling [test (ii)] is tested across densities, mixtures, or shells, while test (v) varies observation noise a via tracer friction or channel precision. Finally, isoconfigurational ensembles[6,44] serve as replicas for Step 1 once grouped by record.

VII. CONCLUSION

This framework establishes a signed, quantitative baseline for dynamical heterogeneity. The fixed-history susceptibility of Eq. (8) is the conditioned analog of the four-point susceptibility $\chi_4(t)$,[51–53] and conditioning can only subtract from it. Interpreting dynamical heterogeneity therefore takes two steps: compute the conditioning-only baseline from the one-path law, then read the susceptibility measured at fixed record as an excess over that baseline. Growth of dynamical heterogeneity on approach to arrest cannot originate in the conditioned sector. It must exceed the negative shield through genuine dynamical correlations, such as recollisions, conserved fields, or critical amplification, and Eq. (11) turns this

© Author(s) 2026

statement into a quantitative threshold against propensity fluctuations that trajectory data can locate with the protocol of Sec. VI A. The theorem covers one tagged population exactly; carrying it to the bulk χ_4, which compares fluctuations across different tagged particles and their cages, requires controlling cross-population correlations and stands as a concrete, well-posed open problem.

ACKNOWLEDGMENTS

This study was supported by the National Human Genome Research Institute of the National Institutes of Health under Award No. R01HG014004. The content is solely the responsibility of the author and does not necessarily represent the official views of the National Institutes of Health.

AUTHOR DECLARATIONS

Conflict of Interest

The author has no conflicts to disclose.

Author Contributions

Hu Cang: Investigation (equal); Project administration (equal); Writing – original draft (equal); Writing – review & editing (equal).

DATA AVAILABILITY

The derivations supporting the findings are contained within the article and its appendices. The simulation and analysis scripts that generate Fig. 5 are available from the author upon reasonable request.

APPENDIX A: THE STOCHASTIC MODEL AND THE CENTERED SQUARE

Let $B, W_1, \ldots, W_z$ be independent Brownian motions. Under the reference law, the system evolves as

$$\begin{aligned} \mathrm{d}X_t &= b_0(X_t)\,\mathrm{d}t + \sigma_0\,\mathrm{d}B_t, \\ \mathrm{d}Y_t^i &= \beta(Y_t^i, X_t)\,\mathrm{d}t + \sigma\,\mathrm{d}W_t^i, \qquad 1 \le i \le z, \end{aligned} \tag{A1}$$

with b_0 and β globally Lipschitz, $\sigma_0, \sigma > 0$, $|f| \le F_*$, hidden initial data independent and identically distributed given X, and a fixed window $[0, T]$; the observation Hilbert space is $L^2([0, T])$. The endogenous law changes only the observed equation, adding the collective drift of Eq. (1). Girsanov's theorem[42] gives the density

$$\exp\left\{\frac{1}{\sigma_0^2}\int_0^T \frac{1}{\sqrt{z}}\sum_{i=1}^{z} f(X_t, Y_t^i)\,[\mathrm{d}X_t - b_0(X_t)\mathrm{d}t] - \frac{1}{2\sigma_0^2}\int_0^T \left[\frac{1}{\sqrt{z}}\sum_{i=1}^{z} f(X_t, Y_t^i)\right]^2 \mathrm{d}t\right\}, \tag{A2}$$

and boundedness of f, giving Novikov's condition (the integrability condition under which the Girsanov factor is a probability density; see, e.g., Ref. 43), so the density is well defined. The linear term is a sum of one-label factors. The quadratic term equals

$$-\frac{1}{2\sigma_0^2 z}\left\|\sum_{i=1}^{z} G_X(Y^i)\right\|^2, \tag{A3}$$

and the $z^{-1/2}$ drift normalization is what makes this coefficient $1/(2az)$ with $a = \sigma_0^2$; an empirical-average drift $z^{-1}\sum_i f$ with order-one output noise would give a z^{-2} coefficient instead, and no order-one shield would survive. Completing the square around the one-path means m_X moves every remaining one-body term into the tilted law Q_X and all constants into the normalization. Explicitly, $\mathrm{d}Q_X/\mathrm{d}R_X(y) \propto \exp\{(a\sqrt{z})^{-1}\int_0^T G_X(y)(t)\,[\mathrm{d}X_t - b_0(X_t)\,\mathrm{d}t] - a^{-1}\langle m_X, G_X(y)\rangle\}$, where R_X is the one-path law under the reference dynamics and $m_X = \mathbb{E}_{Q_X} G_X$ is determined self-consistently. The only term that still couples different labels is

$$-\frac{1}{2az}\left\|\sum_{i=1}^{z}\left(G_X(Y^i) - m_X\right)\right\|^2. \tag{A4}$$

Normalization gives Eq. (2). The derivation explains the sign: once the shared output is fixed, simultaneous motion of all hidden paths along the visible direction receives a quadratic cost. Constants in every remainder quoted in the main text depend only on (F_*, T, a) and are dimension free.

APPENDIX B: LEAVE-TWO-OUT EXPANSION

Write $\widetilde{G}_i = G_X(Y^i) - m_X$ and remove labels 1 and 2 from their sum,

$$W_{z-2} = \frac{1}{\sqrt{z}}\sum_{i=3}^{z}\widetilde{G}_i. \tag{B1}$$

Conditioned on Y^1, Y^2, the remaining integral is the Laplace transform of W_{z-2} evaluated at a field of size $z^{-1/2}(\widetilde{G}_1 + \widetilde{G}_2)$. A second-order expansion around zero gives a two-label density of the form

$$1 - \frac{1}{z}\left\langle \widetilde{G}_1, (aI + C)^{-1}\widetilde{G}_2\right\rangle + O_{L^1}(z^{-3/2}), \tag{B2}$$

where O_{L^1} denotes a remainder whose L^1 norm under the product law is of that order. The one-body pieces are absorbed into the corrected marginals. Multiplying Eq. (B2) by centered observables $u(Y^1)$ and $v(Y^2)$ proves Eq. (6).

The same normal form explains the entropy rate. The leading density perturbation is centered and has size z^{-1}. Relative entropy starts at its quadratic term, so

$$I(Y^1; Y^2 \mid X) = O(z^{-2}). \tag{B3}$$

Covariance is linear in the perturbation and remains $O(z^{-1})$.

APPENDIX C: COLLECTIVE RESUMMATION

Let $U_z = z^{-1/2}\sum_i (u(Y^i) - \mathbb{E}u)$ (the observable $\widetilde{U}_z$ of Sec. IV, here at fixed history). Exchangeability gives

$$\mathrm{Var}\,(U_z) = \mathrm{Var}\,(u) + (z-1)\mathrm{Cov}\,(u_1, u_2). \tag{C1}$$

© Author(s) 2026

Substitute Eq. (6). The factor $z-1$ cancels the pair scale z^{-1} and yields Eq. (8). The correction is finite because all weak pair covariances point along the visible direction.

For the observation variable itself, Gaussian resummation gives

$$D^{-1} = C^{-1} + a^{-1} I, \tag{C2}$$

on the range of C. This expresses precision addition: independent prior fluctuations and observation noise add at the inverse-covariance level. Rearrangement gives Eq. (4).

APPENDIX D: RANDOM HISTORIES

Let $\mathcal{X}$ denote the sigma algebra generated by the observed history. For the normalized collective observable $\widetilde{U}_z = z^{-1/2}\sum_i [u(Y^i) - \mathbb{E}u]$, the law of total variance states,

$$\mathrm{Var}\,(\widetilde{U}_z) = \mathbb{E}[\mathrm{Var}\,(\widetilde{U}_z \mid \mathcal{X})] + \mathrm{Var}\,(\mathbb{E}[\widetilde{U}_z \mid \mathcal{X}]). \tag{D1}$$

The first term contains the single-particle variance minus the Schur shield. In the second, exchangeability gives $\mathbb{E}[\widetilde{U}_z \mid \mathcal{X}] = \sqrt{z}\,[\mu_z(X) - \mathbb{E}\mu_z(X)] = h_z(X)$: the $\sqrt{z}$ amplification of the propensity fluctuation is forced by the normalization of $\widetilde{U}_z$, not chosen. This proves Eq. (10). Applying the same decomposition to two distinct labels gives Eq. (11).

This identity also marks the scope of comparison with a bulk four-point susceptibility. Different ensembles hold different global variables fixed, and those constraints move terms between the two parts of the total variance. A comparison should therefore match the observed history, normalization, and fixed variables before comparing amplitudes.

APPENDIX E: GAUSSIAN CALIBRATION IN FREQUENCY SPACE

For the linear model of Eq. (12), Fourier transformation diagonalizes the path covariance. Observing the complete x history is equivalent to observing $(\partial_t + k_0)x = g\,S + \sqrt{2D_0}\,\eta_0$ with $S = z^{-1/2}\sum_i y_i$ and white noise η_0, so the record's own relaxation rate k_0 drops out of every conditional covariance. Each temporal frequency ω carries the single-particle spectrum

$$C(\omega) = \frac{2\lambda\sigma^2}{\omega^2 + \lambda^2}, \tag{E1}$$

whose integral over $\omega/2\pi$ recovers the stationary variance σ^2. Conditioning adds the observation precision $g^2/2D_0$ at every frequency, so the shielded spectrum is

$$D(\omega) = \frac{aC(\omega)}{a + C(\omega)}, \qquad a = \frac{2D_0}{g^2}, \tag{E2}$$

which is related to $a = 2D_0$ of Sec. V by dividing the record by g, with poles at $\pm i\alpha$, $\alpha^2 = \lambda^2 + g^2\lambda\sigma^2/D_0$. Inverse Fourier transformation produces the two exponential scales in Eq. (13). Evaluating at zero lag gives the equal-time predictable fraction $1 - \lambda/\alpha$. Evaluating at zero frequency gives the integrated fraction $1 - \lambda^2/\alpha^2$.

The difference between these numbers is physically useful. It shows that an observation can strongly constrain slow collective motion while leaving faster fluctuations comparatively free. Any reduced model that replaces the path operator with one static number should state which temporal filter that number calibrates.

APPENDIX F: OVERVIEW OF THEORETICAL RESULTS

Main theoretical results, corresponding equations, proofs, and underlying assumptions.

APPENDIX G: SUMMARY OF NOTATION

Summary of mathematical notation, physical interpretations, and first appearance.

REFERENCES

[1] C. A. Angell, Science **267**, 1924 (1995).
[2] M. D. Ediger, Annu. Rev. Phys. Chem. **51**, 99 (2000).
[3] P. G. Debenedetti and F. H. Stillinger, Nature **410**, 259 (2001).
[4] L. Berthier and G. Biroli, Rev. Mod. Phys. **83**, 587 (2011).
[5] L. Berthier, G. Biroli, J.-P. Bouchaud, L. Cipelletti, D. E. Masri, D. L'Hôte, F. Ladieu, and M. Pierno, Science **310**, 1797 (2005).
[6] A. Widmer-Cooper, P. Harrowell, and H. Fynewever, Phys. Rev. Lett. **93**, 135701 (2004).
[7] L. Berthier and R. L. Jack, Phys. Rev. E **76**, 041509 (2007); arXiv:0706.1044.
[8] H. Tong and H. Tanaka, Phys. Rev. X **8**, 011041 (2018).
[9] E. R. Weeks, J. C. Crocker, A. C. Levitt, A. Schofield, and D. A. Weitz, Science **287**, 627 (2000).
[10] W. K. Kegel and A. van Blaaderen, Science **287**, 290 (2000).
[11] A.-S. Sznitman, *École d'Été de Probabilités de Saint-Flour XIX—1989*, *Lecture Notes in Mathematics* (Springer, Berlin, 1991), Vol. 1464, pp. 165–251.
[12] G. Ben Arous and O. Zeitouni, Ann. Inst. Henri Poincare **35**, 85 (1999).
[13] D. Lacker, Probab. Math. Phys. **4**, 377 (2023); arXiv:2105.02983.
[14] D. Lacker, Electron. J. Probab. **27**, 15 (2022); arXiv:2105.03238.
[15] L. Berthier, G. Biroli, J.-P. Bouchaud, W. Kob, K. Miyazaki, and D. R. Reichman, J. Chem. Phys. **126**, 184503 (2007); arXiv:cond-mat/0609656.
[16] M. Kac, *Proceedings of the Third Berkeley Symposium on Mathematical Statistics and Probability* (University of California Press, Berkeley, 1956), Vol. 3, pp. 171–197.
[17] H. P. McKean, *Stochastic Differential Equations*, *Lecture Series in Differential Equations, Session 7* (Air Force Office of Scientific Research, Arlington, VA, 1967), pp. 41–57.
[18] R. S. Ellis and C. M. Newman, Z. Wahrscheinlichkeitstheorie Verw. Geb. **44**, 117 (1978).
[19] E. Bolthausen, Probab. Theory Relat. Fields **72**, 305 (1986).
[20] S. Kusuoka and S. Liang, Probab. Theory Relat. Fields **116**, 221 (2000).
[21] V. Bally and E. Löcherbach, arXiv:2606.23433 (2026).
[22] J. Jalowy, Z. Kabluchko, and M. Löwe, Math. Phys. Anal. Geom. **28**, 6 (2025); arXiv:2410.08004.
[23] V. Bapst, T. Keck, A. Grabska-Barwińska, C. Donner, E. D. Cubuk, S. S. Schoenholz, A. Obika, A. W. R. Nelson, T. Back, D. Hassabis, and P. Kohli, Nat. Phys. **16**, 448 (2020).
[24] F. S. Pezzicoli, G. Charpiat, and F. P. Landes, SciPost Phys. **16**, 136 (2024); arXiv:2211.03226.
[25] H. Cang, J. Li, V. N. Novikov, and M. D. Fayer, J. Chem. Phys. **118**, 9303 (2003).
[26] H. Cang, J. Li, and M. D. Fayer, Chem. Phys. Lett. **366**, 82 (2002).
[27] H. Cang, J. Li, H. C. Andersen, and M. D. Fayer, J. Chem. Phys. **123**, 064508 (2005).
[28] H. Cang, J. Li, V. N. Novikov, and M. D. Fayer, J. Chem. Phys. **119**, 10421 (2003).
[29] H. Mori, Prog. Theor. Phys. **33**, 423 (1965).
[30] R. Zwanzig, J. Chem. Phys. **33**, 1338 (1960).
[31] W. Götze, *Complex Dynamics of Glass-Forming Liquids: A Mode-Coupling Theory* (Oxford University Press, Oxford, 2009).

© Author(s) 2026

[32]L. M. C. Janssen, Front. Phys. **6**, 97 (2018).
[33]R. van Zon and J. Schofield, Phys. Rev. E **65**, 011106 (2002); arXiv:cond-mat/0108029.
[34]A. Latz, J. Phys.: Condens. Matter **12**, 6353 (2000); arXiv:cond-mat/9911025.
[35]P. Mayer, K. Miyazaki, and D. R. Reichman, Phys. Rev. Lett. **97**, 095702 (2006).
[36]L. M. C. Janssen, P. Mayer, and D. R. Reichman, J. Stat. Mech. **2016**, 054049; arXiv:1510.07636.
[37]C. Luo and L. M. C. Janssen, J. Chem. Phys. **153**, 214507 (2020); arXiv:1909.00428.
[38]V. E. Debets, C. Luo, S. Ciarella, and L. M. C. Janssen, Phys. Rev. E **104**, 065302 (2021); arXiv:2108.06829.
[39]P. Nikolaev, SIAM J. Math. Anal. **57**, 3071 (2025).
[40]L. Li, Y. Wang, and Y. Wang, arXiv:2312.00339 (2025).
[41]S. Albeverio and S. Liang, Ann. Probab. **33**, 300 (2005); arXiv:math/0503601.
[42]I. V. Girsanov, Theory Probab. Appl. **5**, 285 (1960).
[43]B. Øksendal, *Stochastic Differential Equations: An Introduction with Applications*, 6th ed. (Springer, Berlin, 2003).
[44]A. Widmer-Cooper and P. Harrowell, J. Chem. Phys. **126**, 154503 (2007).
[45]G. Biroli and J.-P. Bouchaud, Europhys. Lett. **67**, 21 (2004); arXiv:cond-mat/0401260.
[46]G. Biroli, J.-P. Bouchaud, K. Miyazaki, and D. R. Reichman, Phys. Rev. Lett. **97**, 195701 (2006); arXiv:cond-mat/0605733.
[47]S. Franz, H. Jacquin, G. Parisi, P. Urbani, and F. Zamponi, Proc. Natl. Acad. Sci. U. S. A. **109**, 18725 (2012); arXiv:1206.2482.
[48]S. Särkkä, *Bayesian Filtering and Smoothing* (Cambridge University Press, Cambridge, 2013).
[49]T. G. Mason and D. A. Weitz, Phys. Rev. Lett. **74**, 1250 (1995).
[50]F. Noé and F. Nüske, Multiscale Model. Simul. **11**, 635 (2013).
[51]N. Lačević, F. W. Starr, T. B. Schrøder, and S. C. Glotzer, J. Chem. Phys. **119**, 7372 (2003).
[52]C. Toninelli, M. Wyart, L. Berthier, G. Biroli, and J.-P. Bouchaud, Phys. Rev. E **71**, 041505 (2005).
[53]*Dynamical Heterogeneities in Glasses, Colloids, and Granular Media*, edited by L. Berthier, G. Biroli, J.-P. Bouchaud, L. Cipelletti, and W. van Saarloos (Oxford University Press, Oxford, 2011).

© Author(s) 2026